ADVANCED FUNCTIONAL MATERIALS
www.afm-journal.de

www.MaterialsViews.com

Covalently Tethered Polyoxometalate–Pyrene Hybrids for Noncovalent Sidewall Functionalization of Single-Walled Carbon Nanotubes as High-Performance Anode Material

*Dui Ma, Liying Liang, Wei Chen, Haimei Liu, and Yu-Fei Song**

A covalently tethered polyoxometalate (POM)–pyrene hybrid (Py–SiW_{11}) is utilized for the noncovalent functionalization of single-walled carbon nanotubes (SWNTs). The resulting SWNTs/Py–SiW_{11} nanocomposite shows that both SiW_{11} and pyrene moieties could interact with SWNTs without causing any chemical decomposition. When used as anode material in lithium-ion batteries, the SWNTs/Py–SiW_{11} nanocomposite exhibits higher discharge capacities, and better rate capacity and cycling stability than the individual components. When the current density is 0.5 mA cm^{-2}, the nanocomposite exhibits the initial discharge capacity of 1569.8 mAh g^{-1}, and a high discharge capacity of 580 mAh g^{-1} for up to 100 cycles.

1. Introduction

Polyoxometalates (POMs) represent a diverse range of molecular clusters of V, Mo, W, Nb, and so on, in their highest oxidation state with unmatched range of physical properties such as electronic versatility, redox character, and unique molecular structures, etc.[1,2] Compared with the large number of crystal structures of POMs reported in the literature, the development of POMs-based functional assemblies and materials is one of the most important research fields. Recently, the investigation of the POMs-modified carbon nanotubes (CNTs) became a fascinating topic. For example, Chen and colleagues[3a] reported $H_7PMo_{12}O_{42}$-modified carbon nanotubes as new catalyst support for methanol electro-oxidation. Bonchio and co-workers,[3b] reported efficient water oxidation at the POM-CNTs interface. Giusti et al.[4] reported new assemblies of magnetic POMs on single-walled carbon nanotubes (SWNTs). The group of Yoshikawa and Awaga developed an interesting nanohybrid system of $[PMo_{12}O_{40}]^{3-}$/SWNTs as cathode material with a higher battery capacity and faster charging/discharging properties compared with those molecular cluster batteries.[5]

SWNTs, as a new allotropic form of carbon, show superior and in many cases unique properties.[6] It has been demonstrated that noncovalent sidewall functionalization of SWNTs with polycyclic aromatic compounds such as pyrene proves to be able to improve their dispersion and chemical compatibilities.[7,8] Given the excellent structural and electronic properties of SWNTs, the application of SWNTs as anode material for lithium-ion batteries (LIBs) have been investigated extensively.[9,10] It is known that the LIBs of "purified" SWNTs are generally in the range of 400 and 460 mAh g^{-1},[11] and the attempt to shorten and induce sidewall defects in the SWNTs have resulted in the capacity reaching ≈1000 mAh g^{-1} so far.[12] Nevertheless, the design and development of functional materials that can further increase the capacity remains hard to predict and highly challenging.

Considering that pyrene and its derivatives exhibit strong affinity to SWNTs,[7,8] and POMs could be spontaneously adsorbed onto SWNTs,[13] it is highly interesting to ask a question whether the co-existence of pyrene and POMs can induce more sidewall defects in the SWNTs. Here, covalently tethered a POM–pyrene hybrid with the molecular structure of $(Bu_4N)_4\{(SiW_{11}O_{39})[O(SiCH_2CH_2CH_2NH–COOCH_2C_{16}H_9)_2]\}$ (Py–SiW_{11}) for noncovalent functionalization of SWNTs results in the formation of the SWNTs/Py–SiW_{11} nanocomposite (**Scheme 1**). The investigation of the Py–SiW_{11} modified SWNTs nanocomposite as anode material has been carried out for the first time, exhibiting large enhancement of the discharge capacities, excellent rate capacity, and good cycling stability than the individual components of POM or pyrene.

2. Results and Discussion

Noncovalent functionalization, based on the π–π stacking of the pyrene derivatives with SWNTs, has been widely used to disperse nanotubes,[16] and to combine the nanotubes with photo-/electroactive species[17] and biomolecules.[5,18] Herein, the apolar POM-pyrene hybrid of Py–SiW_{11} is designed to generate both π–π and electrostatic interactions with the SWNTs.

One of the most interesting aspects of POMs lies with the fact that the clusters can be viewed as transferable building blocks. As such, the controlled assembly of POM-based building blocks defines a crucial challenge to engineer the POM building blocks into novel architectures with functionality. An important extension to this building block concept is realized by the use of POMs to form organic/inorganic hybrid

D. Ma, L. Liang, W. Chen, Prof. H. Liu, Prof. Y.-F. Song
Beijing University of Chemical Technology
Beijing 10009, P. R. China
E-mail: songyufei@hotmail.com;
songyf@mail.buct.edu.cn

DOI: 10.1002/adfm.201301624

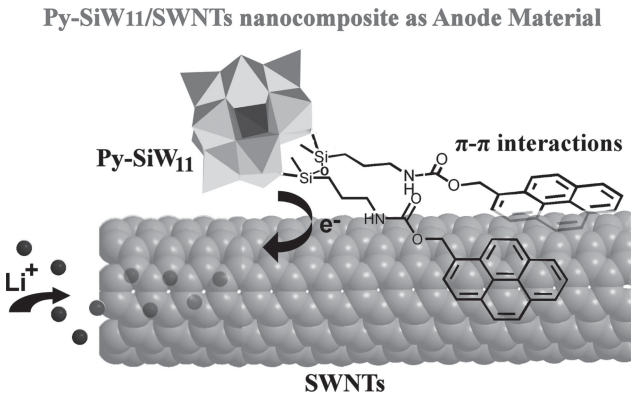

Scheme 1. Schematic description of the SWNTs/Py–SiW_{11} nanocomposite as anode material.

assemblies,[14] which comprise covalently connected cluster and organo fragments. As shown in **Scheme 2**, reaction of the pyren-1-ylmethanol (Py–CH_2OH) with 3-(triethoxysilyl)-propyl isocyanate in the presence of triethylamine (Et_3N) leads to the formation of the pyren-1-ylmethyl-(3-(triethoxysilyl)propyl)-carbamate (Py–$Si(OEt)_3$). Reaction of Py-$Si(OEt)_3$ with the lacunary POM of $K_8[SiW_{11}O_{39}]\cdot 13H_2O$ (SiW_{11})[15] affords new inorganic/organic hybrid assembly with the molecular structure of $(Bu_4N)_4\{SiW_{11}O_{39}[O(Si(CH_2)_3NH–COOCH_2C_{16}H_9)_2]\}$ (Py–SiW_{11}), which has been fully characterized by Fourier transform IR spectroscopy (FTIR), ^1H NMR, ^{13}C NMR, and ^{29}Si NMR (Figures S1–S4, Supporting Information). Electrospray ionization mass spectrometry (ESI-MS) of Py–SiW_{11} shows two signals at m/z 1932 and 1812, which could be assigned to $[(Py–SiW_{11})–2(TBA)^+]^{2-}$ and $[(Py–SiW_{11})–3(TBA)^+ + H^+)]^{2-}$, respectively.

As shown in **Figure 1**a, the presence of chemisorbed SiW_{11} onto SWNTs is evident from FTIR spectrum since the unique bands of both SiW_{11} and SWNTs can be observed in the nanocomposite material. For example, FTIR spectrum of pristine SWNTs displays two weak C–H stretching bands at 2919 and 2848 cm^{-1}, and the aromatic C=C vibration bands at 1653, 1439 cm^{-1}. In contrast, the C–H stretching bands at 2913 and 2842 cm^{-1}, and the C=C vibration at 1656 and 1450 cm^{-1}, respectively, could be observed in the corresponding SWNTs/Py–SiW_{11} nanocomposite. The C=O and Si–O–Si vibration bands shift from 1716 and 1044 cm^{-1} in the Py–SiW_{11} to 1736 and 1044 cm^{-1} in the SWNTs/Py–SiW_{11} nanocomposite, which indicates the interactions between Py–SiW_{11} and SWNTs. Thermogravimetric analysis (TGA) results of SWNTs, Py–SiW_{11}, and SWNTs/Py–SiW_{11} have been presented in Figure 1b. It can be seen that the pristine SWNTs do not exhibit any decomposition before 525 °C, while the Py–SiW_{11} and SWNTs/Py–SiW_{11} nanocomposites show the weight loss of 31.2 and 13.2 wt%, respectively. If a similar weight-loss behavior of Py–SiW_{11} and SWNTs is assumed to take place,[19,20] the Py–SiW_{11} content in the SWNTs/Py–SiW_{11} nanocomposite can be roughly determined to be 42.3 wt%.

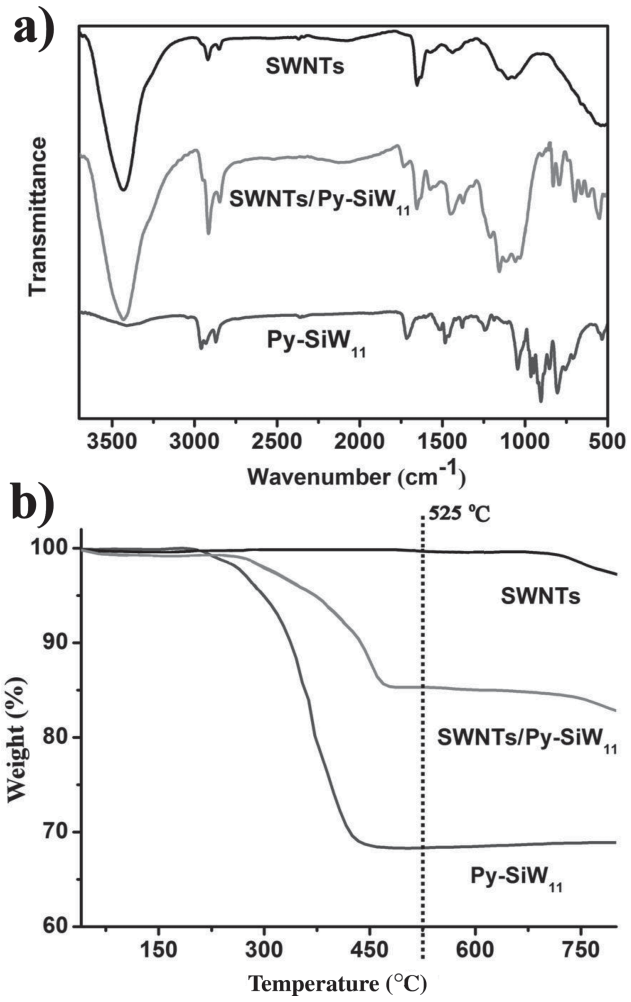

Figure 1. a) FTIR spectra of the pristine SWNTs, SWNTs/Py-SiW_{11}, and Py-SiW_{11}. b) TGA measurements of pristine SWNTs, SWNTs/Py–SiW_{11}, and Py-SiW_{11} in N_2 (10 °C min^{-1}).

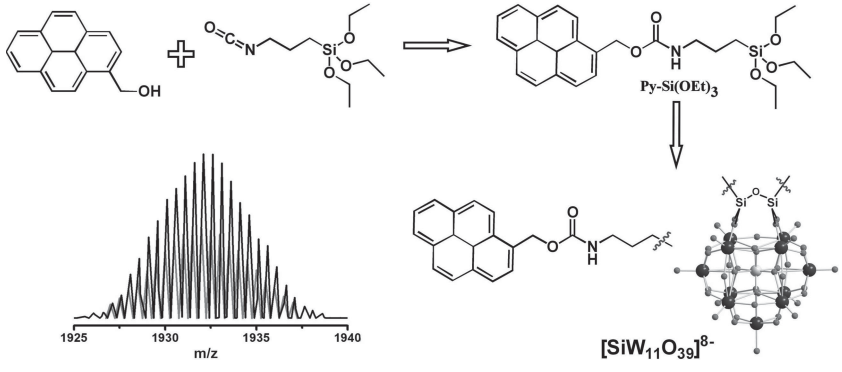

Scheme 2. The synthetic pathway for the preparation of covalently functionalized Py–SiW_{11}.

Further characterization of the SWNTs/Py–SiW_{11} nanocomposite has been studied by Raman spectra excited at 633 nm. As shown in **Figure 2**a, the tangential vibration

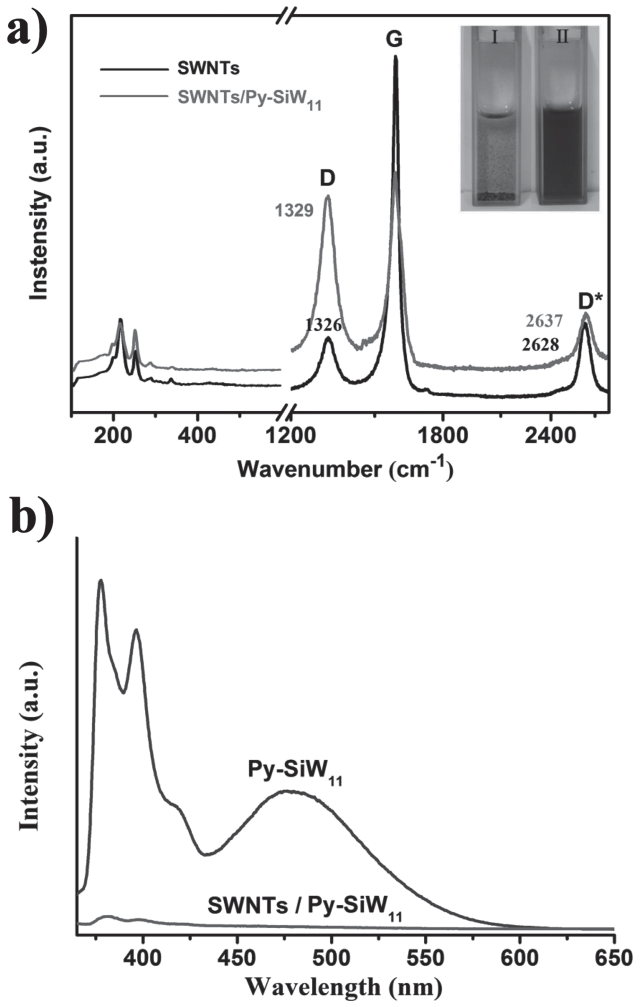

Figure 2. a) Raman spectra of the purified SWNTs and SWNTs/Py–SiW_{11}, respectively; excitation $\lambda = 633$ nm. Inset: photographs of the DMF solution of I) pristine SWNTs and II) SWNTs/Py–SiW_{11}. b) Fluorescence spectra of Py–SiW_{11} and SWNTs/Py–SiW_{11} in dimethylformamide (DMF): $\lambda_{ex} = 344$ nm.

mode (G band)[20] at 1586 cm^{-1} is clearly observed for both SWNTs and SWNTs/Py–SiW_{11} nanocomposite. Meanwhile, the disorder-induced D band shifts slightly from 1326 in SWNTs to 1329 cm^{-1} in SWNTs/Py–SiW_{11}. Contrast experiment shows that no Raman absorption can be observed at ≈1300 cm^{-1} for Py–SiW_{11} alone. Moreover, it is noted that Raman spectra of SWNTs/Py–SiW_{11} exhibit a D mode with similar intensity to the high-energy G mode, whereas the intensity of D band is much lower than that of G band in pristine SWNTs. Such result in the SWNTs/Py–SiW_{11} nanocomposite could be attributed to the dislocation of more surface defects of SWNTs under the experimental conditions. The second disordered D^* band shift significantly to higher frequency from 2628 in SWNTs to 2637 cm^{-1} in SWNTs/Py–SiW_{11} nanocomposite. The shift of D band to higher frequency indicates the loss of electrons on SWNTs, and the presence of the intermolecular interactions between SWNTs and Py–SiW_{11}.[21]

The fluorescence spectroscopy provides proof for the interactions between Py–SiW_{11} and SWNTs. Pyrene is a well-known

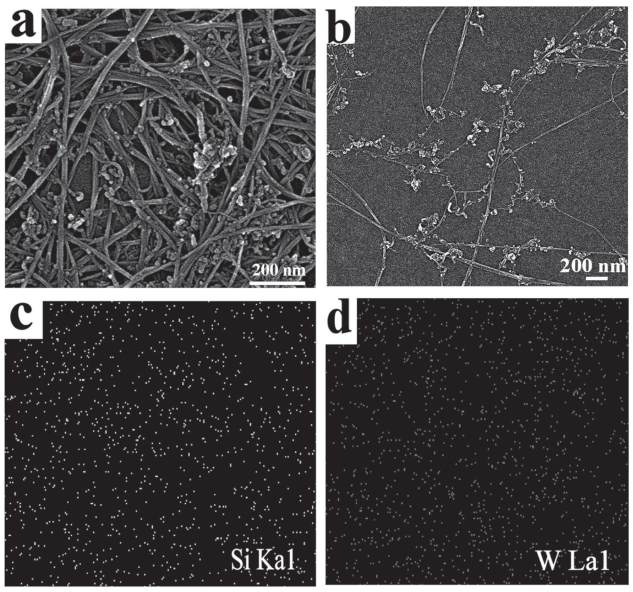

Figure 3. SEM images of a) the pristine SWNTs and b) SWNTs/Py–SiW_{11} nanocomposite. c,d) EDX elemental maps of SWNTs/Py–SiW_{11} nanocomposite.

luminophore and its dilute and concentrated solutions exhibit monomer and excimer emissions in the UV and visible regions, respectively.[20,22] The steady-state fluorescence emission spectrum of Py–SiW_{11} shows two monomer emission at 377 and 396 nm, and one excimer emission at 476 nm. In contrast, the emission spectrum of the SWNTs/Py–SiW_{11} nanocomposite is almost completely quenched, which indicates that the decay of singlet excited pyrene moieties is affected by their binding to SWNTs. In other words, the emission quenching of the SWNTs/Py–SiW_{11} nanocomposite may be caused by the pronounced electron and/or energy transfer between Py–SiW_{11} and SWNTs since it is well-known that SWNTs are non-emissive.[21]

Figure 3 exhibits scanning electron microscopy (SEM) images of the Py–SiW_{11}/SWNTs nanocomposite and the pristine SWNTs as control. It can be seen that the agglomeration of SWNTs is clearly visible in the SEM images of pristine SWNTs. In contrast, the SWNTs bundles are found to be loosened upon treatment with Py–SiW_{11}, which indicates the improved dispersion of SWNTs in the nanocomposite sample. To confirm the formation of the SWNTs/Py–SiW_{11} nanocomposite, the spatial distribution of metal elements in the SWNTs/Py–SiW_{11} nanocomposite has been examined using energy-dispersive X-ray (EDX) elemental mapping analysis. As illustrated in Figure 3c,d, the silicon and tungsten are homogeneously distributed in the SWNTs/Py–SiW_{11} nanocomposite materials.

Transmission electron microscopy (TEM) images of pristine SWNTs do not reveal any externally grafted objects (Figure S6, Supporting Information). In contrast, TEM images of the SWNTs/Py–SiW_{11} nanocomposite show the presence of bundles decorated by dark spots that can be clearly distinguished as Py–SiW_{11} by EDX measurement (Figure S6, Supporting Information), which confirms the presence of tungsten, silicon, and potassium (the peak for copper is ascribed to the used copper grids). High resolution (HR) TEM images

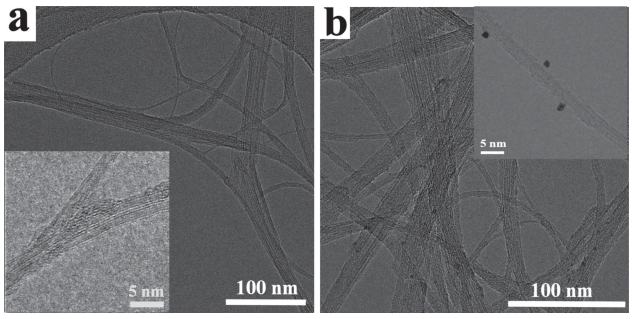

Figure 4. HRTEM images of a) the pristine SWNTs and b) SWNTs/Py–SiW_{11} nanocomposite.

(**Figure 4**) of the SWNTs/Py–SiW_{11} nanocomposite suggest that the grafted objects (the dark spots) possess a diameter of about 1–1.5 nm, which is in good agreement with the size of Py–SiW_{11}. This result indicates that the individual Py–SiW_{11} molecules have been attached to the surface of the SWNTs.

Electrochemical properties of the SWNTs/Py–SiW_{11} nanocomposite as anode material for lithium-ion batteries have been investigated. **Figure 5** shows the charge–discharge voltage profiles of the SWNTs/Py–SiW_{11} nanocomposite and Py–SiW_{11}

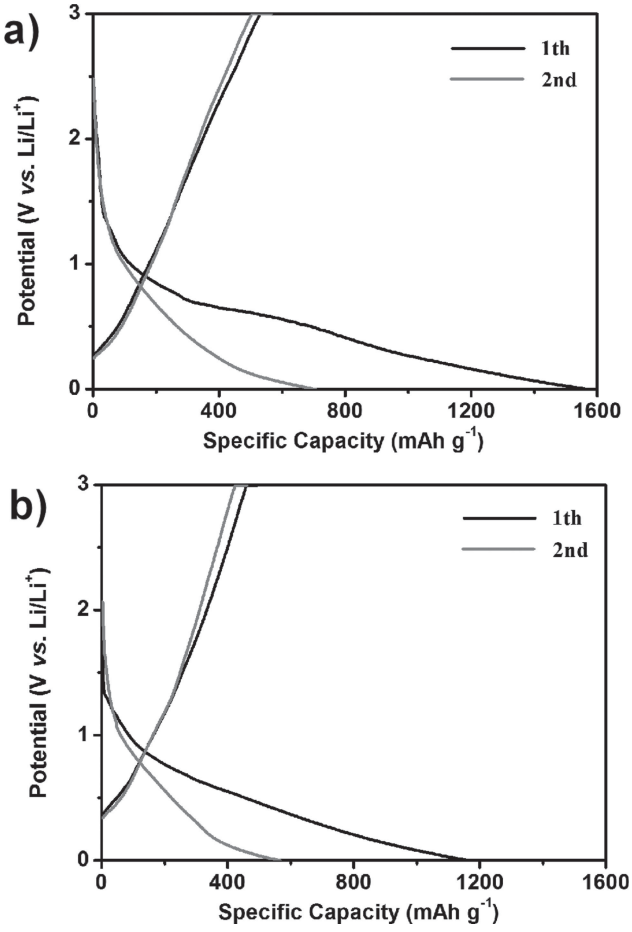

Figure 5. First and second charging and discharging curves of the lithium rechargeable battery; current density was 0.5 mA cm^{-2}: a) SWNTs/Py–SiW_{11} electrode and b) Py–SiW_{11} electrode.

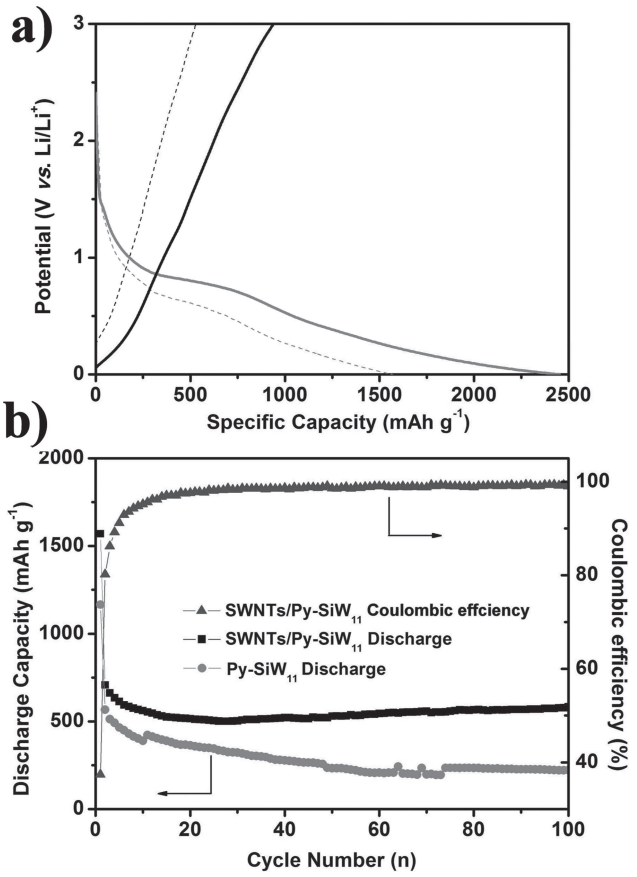

Figure 6. a) First charging (up) and discharging (down) curves of the SWNTs/Py–SiW_{11} with current densities of 0.1 mA (solid line) and 0.5 mA cm^{-2} (dashed line). b) Discharge capacity and Coulombic efficiency vs cycle number; current density was 0.5 mA cm^{-2}.

electrode with the current density of 0.5 mA cm^{-2} for the first two cycles. The first discharge capacity of the SWNTs/Py–SiW_{11} and Py–SiW_{11} electrode are 1569.8 mAh g^{-1} and 1165.9 mAh g^{-1}, and in the second cycle, the discharge capacities of 707.1 and 566.6 mAh g^{-1} have been achieved, respectively. The above results reveal that the SWNTs/Py–SiW_{11} electrode has a bigger specific capacity than the individual components of Py–SiW_{11} or SWNTs electrode, which indicates that noncovalent functionalization of SWNTs by Py–SiW_{11} leads to the large enhancement of the performance as anode material when compared with SWNTs. It should be noted that for both SWNTs/Py–SiW_{11} and Py–SiW_{11} electrodes, the specific capacities decrease in the first two cycles due to some irreversible surface reactions on both electrodes. However, the capacities remain stable up to 100 cycles after the 2nd cycle.

Figure 6a shows the first charge–discharge curves of the SWNT/Py–SiW_{11} nanocomposite at the current densities of 0.1 and 0.5 mA cm^{-2}, respectively. It is observed that the initial discharge specific capacity of the SWNTs/Py–SiW_{11} nanocomposite increases from 1569.8 to 2453 mAh g^{-1} with the decrease of the current density from 0.5 to 0.1 mA cm^{-2}, and the capacity retention is as high as 64%. Figure 6b shows the cycling stability and capacity retention of the SWNTs/Py–SiW_{11}

and Py–SiW_{11} electrode at the current density of 0.5 mA cm^{-2}. For the SWNTs/Py–SiW_{11} nanocomposite, the first discharge capacity is 1569.8 mAh g^{-1}, and then it exhibits the capacity decay from the second cycle. After 20 cycles, the capacity remains stable and a capacity of 580 mAh g^{-1} could be achieved after 100 cycles, with high capacity retention of 37%. In contrast, the reversible capacity of the bare Py–SiW_{11} electrode drops rapidly from the 20th cycle at 0.5 mA cm^{-2}, and after 100 cycles, the capacity retention is just 19%. Such a prominent difference between SWNTs/Py–SiW_{11} and bare Py–SiW_{11} highlights the efficiency of the SWNTs/Py–SiW_{11} nanocomposite material as high-performance anode material.

High electrode reversibility is another very important parameter for practical battery applications. Although the first Coulombic efficiency of the SWNTs/Py–SiW_{11} nanocomposite is only 37.4%, those of the following cycles are up to 99%. The above results suggest that the SWNTs/Py–SiW_{11} nanocomposite shows a much better cycle stability than that of bare Py–SiW_{11} electrode. This is because that the sidewall defects of SWNTs, due to the noncovalent functionalization of Py–SiW_{11}, shorten the diffusion length of lithium ions and enable effective electrolyte transport.

The rate performance and the cycling stability during the lithium ion insertion/extraction processes are key factors for practical application. Herein, the rate capability of SWNTs/Py–SiW_{11} has been evaluated at various currents in the range of 0.05–1 mA cm^{-2} at the cut-off voltage between 0 and 3.0 V Li^+/Li, and the results are presented in **Figure 7**a. The discharge capacities of 920, 775, and 640 mA h g^{-1} have been obtained at the current densities of 0.05, 0.1, and 0.2 mA cm^{-2}, respectively. The capacities at a higher current of 1 mA cm^{-1}, although, fading rapidly, could still deliver 360 mAh g^{-1}. Moreover, even after 70 cycles, when the current is restored to 0.05 mA cm^{-2}, the SWNTs/Py–SiW_{11} nanocomposite delivers 950 mAh g^{-1} without fading. The stable cycle performance of the SWNTs/Py–SiW_{11} nanocomposite at high rates indicates the ultra-fast solid-state diffusion of Li ions in bulk owing to the short diffusion path length and stable structure.

Figure 7b shows the cyclic voltammograms of the SWNTs/Py–SiW_{11} nanocomposite at a scan rate of 0.1 mV s^{-1} over the range of 0–3 V. In the first cycle, an irreversible reduction peak at about 0.7 V indicates the formation of solid electrolyte interphase (SEI), however, this peak disappears in the following cycles. The peak of 0.01–0.2 V in the reduction process is caused by the insertion of Li. The oxidation peak at ≈0.2 V shown in the charge process can be ascribed to the Li-extraction from the SWNTs. Such Li-extraction process could be observed in the following cycles, suggesting the good reversibility of the SWNTs/Py–SiW_{11} nanocomposite.

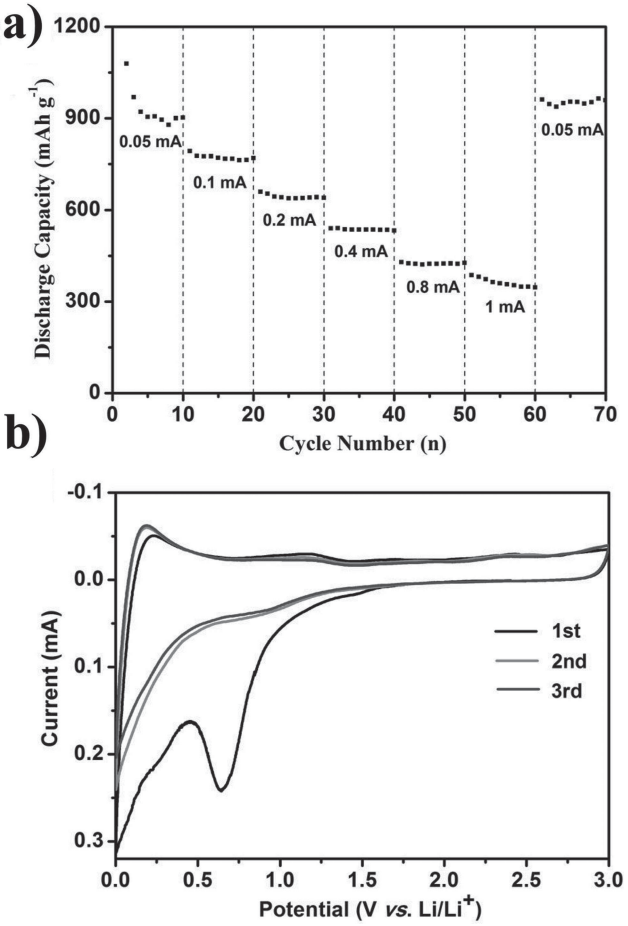

Figure 7. a) Rate performance of the SWNTs/Py–SiW_{11} composite electrode at various current densities of 0.05, 0.1, 0.2, 0.4, 0.8, and 1 mA cm^{-2}. b) Cyclic voltammograms for SWNTs/Py–SiW_{11} with a scan rate of 0.1 mV s^{-1} in the potential range 0–3 V.

3. Conclusions

The noncovalent sidewall functionalization of SWNTs by a covalently modified POM-pyrene hybrid of Py-SiW_{11} has been carried out for the first time. The experimental results suggest that the Py–SiW_{11} modified SWNTs results in the quench of the emission spectrum, which might be due to the electron and energy transfer between Py–SiW_{11} and SWNTs. The SWNTs/Py–SiW_{11} nanocomposite exhibits a high discharge capacity of 580 mAh g^{-1} for up to one hundred cycles, with a relatively stable performance at a current density of 0.5 mA cm^{-2}. The excellent electrochemical performance can be attributed to the sidewall defects of SWNTs by introducing Py–SiW_{11}, which shorten the diffusion length of lithium ions and enable effective electrolyte transport. Further investigation of the application of such SWNTs/Py–SiW_{11} nanocomposite is in progress.

Supporting Information

Supporting Information is available from the Wiley Online Library or from the author.

Acknowledgements

Financial support from National Science Foundation of China (21222104, 21076020), the Beijing Nova Program (2009B12), the Fundamental Research Funds for the Central Universities (ZZ1227).

Received: May 12, 2013
Revised: June 5, 2013
Published online: July 8, 2013

[1] a) C. L. Hill, *Chem. Rev.* **1998**, *98*; b) L. Cronin, A. Müller, *Chem. Soc. Rev.* **2012**, *41*, 7333–7334; c) D. L. Long, E. Burkholder, L. Cronin, *Chem. Soc. Rev.* **2007**, *36*, 105–121; d) Y. F. Song, D. L. Long, C. Ritchie, L. Cronin, *Chem. Rec.* **2011**, *11*, 158–171; e) A. Dolbecq, E. Dumas, C. R. Mayer, P. Mialane, *Chem. Rev.* **2010**, *110*, 6009–6048; f) A. Müller, P. Gouzerh, *Chem. Soc. Rev.* **2012**, *41*, 7431–7463; g) C. Pan, D. Li, T. Liu, *Chem. Soc. Rev.* **2012**, *41*, 7368–7383; h) A. Proust, B. Matt, R. Villanneau, G. Guillemot, P. Gouzerh, G. Izzet, *Chem. Soc. Rev.* **2012**, *41*, 7605–7622; i) S. T. Zheng, G. Yang, *Chem. Soc. Rev.* **2012**, *41*, 7623–7646; j) Y. F. Song, R. Tsunashima, *Chem. Soc. Rev.* **2012**, *41*, 7384–7402.

[2] a) D. Li, J. Song, P. Yin, S. Simotwo, A. Bassler, Y. Aung, J. E. Roberts, K. I. Hardcastle, C. L. Hill, T. Liu, *J. Am. Chem. Soc.* **2011**, *133*, 14010–14016; b) T. Liu, E. Diemann, H. Li, A. W. M. Dress, A. Müller, *Nature.* **2003**, *426*, 59–62; c) Y. F. Song, N. McMillan, D. L. Long, S. Kane, J. Malm, M. O. Riehle, C. P. Pradeep, N. Gadegaard, L. Cronin, *J. Am. Chem. Soc.* **2009**, *131*, 1340–1341; d) B. Keita, L. Nadjo, *Encyclopedia of Electrochemistry*, Vol. *7* (Eds: A. J. Bard, M. Stratmann), Wiley-VCH, Weinheim **2006**, pp 607–700; e) J. Zhang, Y. F. Song, L. Cronin, T. Liu, *J. Am. Chem. Soc.* **2008**, *130*, 14408–14409.

[3] a) D. Pan, J. Chen, W. Tao, L. Nie, S. Yao, *Langmuir.* **2006**, *22*, 5872–5876; b) F. M. Toma, A. Sartorel, M. Iurlo, M. Carraro, P. Parisse, C. Maccato, S. Rapino, B. R. Gonzolez, H. Amenitsch, T. D. Ros, L. Casalis, A. Goldoni, M. Marcaccio, G. Scorrano, G. Scoles, F. Paolucci, M. Prato, M. Bonchio, *Nat. Chem.* **2010**, *2*, 826–831.

[4] a) A. Giusti, G. Charron, S. Mazerat, J. D. Compain, P. Mialane, A. Dolbecq, E. Rivière, W. Wernsdorfer, R. N. Biboum, B. Keita, L. Nadjo, A. Filoramo, J. P. Bourgoin, T. Mallah, *Angew. Chem.* **2009**, *121*, 5049–5052; *Angew. Chem. Int. Ed.* **2009**, *48*, 4949–4952; b) G. Charron, A. Giusti, S. Mazerat, P. Mialane, A. Gloter, F. Miserque, B. Keita, L. Nadjo, A. Filoramo, E. Rivière, W. Wernsdorfer, V. Huc, J. P. Bourgoin, T. Mallah, *Nanoscale* **2010**, *2*, 139–144.

[5] a) N. Kawasaki, H. Wang, R. Nakanishi, S. Hamanaka, R. Kitaura, H. Shinohara, T. Yokoyama, H. Yoshikawa, K. Awaga, *Angew. Chem.* **2011**, *123*, 3533–3536; *Angew. Chem. Int. Ed.* **2011**, *50*, 3471–3474; b) H. Wang, S. Hamanaka, Y. Nishimoto, S. Irle, T. Yokoyama, H. Yoshikawa, K. Awaga, *J. Am. Chem. Soc.* **2012**, *134*, 4918–4924.

[6] a) C. T. White, T. N. Todorov, *Nature* **1998**, *393*, 240–242; b) T. Rueckes, K. Kim, E. Joslelevich, G. Y. Tseng, C. L. Cheung, C. M. Lieber, *Science* **2000**, *289*, 94–97; c) M. F. Yu, O. Lourie, M. J. Dyer, K. Moloni, T. F. Kelly, R. S. Ruoff, *Science* **2000**, *287*, 637–640; d) D. A. Britz, A. N. Khlobystov, *Chem. Soc. Rev.* **2006**, *35*, 637–659; e) M. Iurlo, D. Paolucci, M. Marcaccio, F. Paolucci, *Chem. Commun.* **2008**, 4867–4874; f) F. D'Souza, O. Ito, *Chem. Commun.* **2009**, 4913–4928; g) K. Y. Tomizaki, T. Kurosawa, M. Kajiyama, T. Imai, *Chem. Lett.* **2012**, *41*, 597–599; h) M. Ertas, R. M. Walczak, R. K. Das, A. G. Rinzler, J. R. Reynolds, *Chem. Mater.* **2012**, *24*, 433–443.

[7] R. J. Chen, Y. Zhang, D. Wang, H. Dai, *J. Am. Chem. Soc.* **2001**, *123*, 3838–3839.

[8] L. Liu, T. Wang, J. Li, Z. X. Guo, L. Dai, D. Zhang, D. Zhu, *Chem. Phys. Lett.* **2003**, *367*, 747–752.

[9] D. Deng, M. G. Kim, J. Y. Lee, J. Cho, *Energy Environ. Sci.* **2009**, *2*, 818–837.

[10] a) C. Ban, Z. Wu, D. T. Gillaspie, L. Chen, Y. Yan, J. L. Blackburn, A. C. Dillon, *Adv. Mater.* **2010**, *22*, 145–149; b) I. Lahiri, S. W. Oh, J. Y. Hwang, S. Cho, Y. K. Sun, R. Banerjee, W. Choi, *ACS Nano* **2010**, *4*, 3440–3446.

[11] a) A. S. Claye, J. E. Fischer, C. B. Huffman, A. G. Rinzler, R. E. Smalley, *J. Electrochem. Soc.* **2000**, *147*, 2845–2852; b) E. Frackowiak, F. Beguin, *Carbon* **2002**, *40*, 1775–1787; c) S. H. Ng, J. Wang, Z. P. Guo, J. Chen, G. X. Wang, H. K. Liu, *Electrochim. Acta.* **2005**, *51*, 23–28.

[12] B. J. Landi, M. J. Ganter, C. M. Schauerman, C. D. Cress, R. P. Raffaelle, *J. Phys. Chem. C.* **2008**, *112*, 7509–7515.

[13] B. Fei, H. Lu, Z. Hu, J. H. Xin, *Nanotechnology* **2006**, *17*, 1589–1593.

[14] a) Y. F. Song, D. L. Long, L. Cronin, *Angew. Chem.* **2007**, *119*, 3974–3978; *Angew. Chem. Int. Ed.* **2007**, *46*, 3900–3904; b) Y. F. Song, N. McMilla, D. L. Long, J. Thiel, Y. Ding, H. Chen, N. Gadegaard, L. Cronin, *Chem. Eur. J.* **2008**, *14*, 2349–2354; c) J. Thiel, D. Yang, M. H. Rosnes, X. Liu, C. Yvon, S. E. Kelly, Y. F. Song, D. L. Long, L. Cronin, *Angew. Chem.* **2011**, *123*, 9033–9037; *Angew. Chem. Int. Ed.* **2011**, *50*, 8871–8875; d) Y. F. Song, D. L. Long, S. E. Kelly, L. Cronin, *Inorg. Chem.* **2008**, *47*, 9137–9139; e) Y. F. Song, P. J. Kitson, D. L. Long, A. D. C. Parenty, R. J. Thatcher, L. Cronin, *CrystEngComm* **2008**, *10*, 1243–1251.

[15] A. Teze, G. Herve, *J. Inorg. Nucl. Chem.* **1977**, *39*, 999–1002.

[16] M. Lebrón-Colón, M. A. Meador, J. R. Gaier, F. Solá, D. A. Scheiman, L. S. McCorkle, *Appl. Mater.* **2010**, *2*, 669–676.

[17] a) C. Ehli, G. M. A. Rahman, N. Jux, D. Balbinot, D. M. Guldi, F. Paolucci, M. Marcaccio, D. Paolucci, M. Melle-Franco, F. Zerbetto, S. Campidelli, M. Prato, *J. Am. Chem. Soc.* **2006**, *128*, 11222–11231; b) J. Bartelmess, B. Ballesteros, K. D. Gema de la Torre, S. Campidelli, M. Prato, T. Torres, D. M. Guldi, *J. Am. Chem. Soc.* **2010**, *132*, 16202–16211.

[18] A. Knyazev, L. Louise, M. Veber, D. Langevin, A. Filoramo, A. Prina-Mello, S. Campidelli, *Chem. Eur. J.* **2011**, *17*, 14663–14671.

[19] Y. Yan, S. Yang, J. Cui, L. Jakisch, P. Pötschke, B. Voit, *Polym. Int.* **2011**, *60*, 1425–1433.

[20] W. Z. Yuan, Y. Mao, H. Zhao, J. Z. Sun, H. P. Xu, J. K. Jin, Q. Zheng, B. Z. Tang, *Macromolecules* **2008**, *41*, 701–707.

[21] a) A. M. Rao, P. C. Eklund, S. Bandow, A. Thess, R. E. Smalley, *Nature* **1997**, *388*, 257–259; b) J. Zou, L. Liu, H. Chen, S. I. Khondaker, R. D. McCullough, Q. Huo, L. Zhai, *Adv. Mater.* **2008**, *20*, 2055–2060.

[22] a) F. D'Souza, A. S. D. Sandanyaka, O. Ito, *J. Phys. Chem. Lett.* **2010**, *1*, 2586–2593; b) M. Li, P. Xu, J. Yang, H. Ying, K. Haubner, L. Dunsch, S. Yang, *J. Phys. Chem. C.* **2011**, *115*, 4584–4593.